European Journal of Radiology 113 (2019) 204–208

Contents lists available at ScienceDirect

European Journal of Radiology

journal homepage: www.elsevier.com/locate/ejrad

Research article

Differentiation of liver abscess from liver metastasis using dual-energy spectral CT quantitative parameters

Nan Wang[a], Ye Ju[a], Jingjun Wu[a], Ailian Liu[a,*], Anliang Chen[a], Jinghong Liu[a], Yijun Liu[a], Jianying Li[b]

[a] The First Affiliated Hospital of Dalian Medical University, Department of Radiology, Dalian, China
[b] GE Healthcare

ARTICLE INFO

Keywords:
Liver abscess
Liver metastasis
Differential diagnosis

ABSTRACT

Objective: To explore the value of single source dual-energy spectral CT quantitative parameters in differential diagnosis of liver abscess and liver metastatic tumor.

Methods: Fifty-one patients with 73 liver lesions (28 liver abscesses and 45 liver metastases) underwent plain and contrast-enhanced spectral CT scans. The fat and blood concentrations and CT values of 40–140 keV monochromatic images were measured to calculate effective atomic number (Eff-Z) and a slope (K): [CT(40 keV)-CT(140 keV)/100] for the cystic component on the plain scan images. The iodine concentration of the lesion wall on the enhanced three-phase images were measured and normalized to that of aorta for normalized iodine concentration (NIC). All of the single quantitative parameters were compared between liver abscesses and liver metastases by the independent samples *t*-test or Mann-Whitney *U* test. Statistical difference parameters between liver abscesses and liver metastases were analyzed by receiver-operating characteristic (ROC) curves. The diagnostic capability was determined by calculating the area under the curve (AUC). Using binary logistics regression analysis combining the best diagnostic performance parameter in the plain and enhanced phase images. The predictive model of liver abscess was established, and the receiver operating characteristic (ROC) analysis was performed.

Results: There were significant differences in CT value, the slope (K), Eff-Z, blood and fat concentrations in the plain phase and NIC in the contrast-enhanced venous and delay phases between liver abscesses and liver metastases (all $P < 0.05$). The CT value at 40 keV in the plain phase provided 0.761 in area under the curve (AUC) in ROC with sensitivity of 71.4% and, specificity of 75.6% in differentiating liver abscess and tumor. Combining with NIC in delay phase, the respectively values improved to 0.963, and 89.3% and 93.3%.

Conclusion: The quantitative parameters in single source dual-energy CT provide high diagnostic accuracy in differentiating liver abscesses from liver metastases.

1. Introduction

Liver abscess is a serious abdominal infection that may be caused by bacteria, fungi, or parasites. Pathologically, necrosis and liquefaction happened in the liver parenchyma, and then aggregation to form pus cavity. The typical imaging findings of liver abscess on multiphase contrast-enhanced CT are well known, such as the “double target sign” in liver abscess, multilocular appearance, small bubbles or gas-liquid plane in the cavity [1,2]. Atypical liver abscess shows the enhancement of internal septa or multi-circumferential enhancement in lesions. It’s difficult to diagnosis atypical liver abscess accurately. The liver is supplied by the hepatic artery and the portal vein, which provides a very good environment for cancer cells to grow in the liver. Liver metastasis shows a lower density area in the hypodense focus, thus presenting a concentric circular or double contour structure, and edge enhancement due to the hoof tissue at the margin of the tumor, inflammatory cell invasion and vascular proliferation. Further, liver metastasis that develop central necrosis or cyst may mimic the appearance of liver abscess. It’s difficult to diagnose the two types of lesions by using traditional single-energy CT.

Abbreviations: NIC, normalized iodine concentration; Eff-Z, effective atomic number; AUC, area under the curve; MRI, magnetic resonance imaging; ROC, receiver operating characteristic; ROI, region of interest; GSI, gemstone spectral imaging

* Corresponding author at: The First Affiliated Hospital of Dalian Medical University, Department of Radiology, Xigang District, Zhongshan Road, No. 222, Dalian, China.

E-mail address: cjr.liuailian@vip.163.com (A. Liu).

https://doi.org/10.1016/j.ejrad.2019.02.024
Received 12 December 2018; Received in revised form 30 January 2019; Accepted 17 February 2019

MRI has the characteristics of multi-azimuth, multi-direction and multi-parameter, which plays an important role in the diagnosis of liver abscess and liver metastasis. Previous studies [3,4] have shown that diffusion weighted imaging is available in the differential diagnosis between liver abscess and liver metastasis. On the other hand, dual-energy spectral CT imaging based on the rapid switching between 140 and 80 kVp allows the reconstruction of both the monochromatic images with energies ranging from 40 to 140 keV, and the material decomposition images [5] to enable multi-parameter analysis of clinical diagnosis. This imaging method has found use in several clinical applications including differentiating metastases from adenoma in adrenal glands [6] and differentiating liver abscess from cholangiocarcinoma or necrotic hepatocellular carcinoma [7].

The role of MRI in the diagnosis of liver abscess has been discussed in previous studies [3,8], but the use of dual-energy spectral CT imaging in the differential diagnosis between liver abscess and liver metastasis has not been reported. The purpose of the present study was to explore the value of dual-energy spectral CT quantitative parameters in the differential diagnosis between liver abscess and liver metastasis.

2. Materials and methods

2.1. Patients

Retrospective analysis of patients with liver abscesses and liver metastases examined between September 2011 and Dec 2016 was performed. We used the following inclusion criteria to collect 70 patients: (a) patients who underwent dual-energy spectral CT scans with gemstone spectral imaging (GSI) mode; (b) liver abscesses were confirmed by percutaneous drainage or combined with clinical symptom and imaging after follow-up CT imaging at least 1 month; (c) liver metastases were confirmed by medical history and follow-up CT imaging at least 1 month. (d) All the lesions had obvious liquefaction area. Using these criteria, 19 patients were excluded: because (a) patients only underwent plain scan (14 cases). (b) patients had drainage tubes or a lot of gas in the lesions (5 cases). Finally, 25 liver abscess patients (14 men, 11 women; median age 61 years; 33–81 years) with 28 lesions and 26 liver metastasis patients (15 men, 11 women; median age 62 years; 35–86 years) with 45 lesions were included in the study. The primary tumors were colorectal cancer (n = 9), gastric cancer (n = 5), pancreatic cancer (n = 5), lung cancer (n = 3), carcinoma of gallbladder (n = 1), renal carcinoma (n = 1), carcinoma of fallopian tube (n = 1) and mammary cancer (n = 1). The general information of patients are shown in Table 1.

2.2. CT examinations

All patients underwent the plain and three-phase contrast-enhanced CT examinations and scans were performed on a Discovery CT750 HD CT scanner (GE Healthcare, Waukesha, WI). Dual-energy spectral CT imaging was performed in a dorsal position with the following scan parameters: rapid switching of 140 and 80 kVp tube voltage in 0.5 ms, tube current, 375 mA; slice thickness, 5 mm; slice interval, 5 mm; and helical pitch, 1.375. Conventional scanning was performed first, then the GSI mode was used for the contrast-enhanced scan. A high pressure injector was used to inject the contrast agent (Ioversol; 320 mg I/mL) via the cubital vein at a flow rate of 2.0–2.5 mL/s at a dosage of 1.0 mL/kg body weight. Arterial phase, venous phase, and equilibrium phase contrast-enhanced images were obtained 28, 55, and 120 s, respectively, after contrast agent injection. 101 sets of virtual monochromatic images with photon energy levels from 40 to 140 keV, and material decomposition images were reconstructed at 5 mm image slice thickness.

2.3. Qualitative analyses

Two experienced radiologists (observer 1 and observer 2, with 5 and 11 years of experience in abdominal CT imaging, respectively) qualitatively reviewed the 70 keV monochromatic CT images (5-mm thick) by consensus on the PACS. Neither observer was aware of clinical, surgical, and pathologic findings. CT imaging were evaluated for enhancement and morphologic features of the lesions. The observers documented the following morphologic features: (a) the location of lesions; (b) the shape of lesions; (c) double target sign; (d) transient segmental enhancement around the lesion; (e) enhancement pattern of lesions.

2.4. Quantitative analyses

All images were transferred to an Advanced Workstation 4.5 (AW4.5; GE Healthcare) and evaluated quantitatively by an abdominal radiologist (with 5 years of experience) using a GSI viewer software. On the 70 keV monochromatic image of 5 mm slice thickness in the plain CT scan, a region-of-interest (ROI), occupied two-thirds of the cavity area, was placed on the cyst at the image slice containing the largest lesion. The ROI data, including the CT values from 40 keV to 140 keV, Eff-Z, blood (water) concentration and fat (water) concentration, were saved in an EXCEL file. The slope (K) of the spectral HU curve (CT value as function of photon energy from 40 to 140 keV) was calculated with the following formula: K = y/x, where y is the difference between the mean CT value at 40 and 140 keV, and x is the energy level difference (x = 100 in our study). On the meterial decomposition image of 5 mm slice thickness in the contrast-enhanced CT scans, the ROI was placed in the walls of the lesions and the aorta of the coeliac trunk to get the iodine (water) concentration of the walls and the aorta. Normalized iodine concentration (NIC) was derived from the iodine (water) concentration, calculated as $NIC = IC_{lesion}/IC_{aorta}$, where IC_{lesion} and IC_{aorta} are the iodine (water) concentration in the lesions and in the aorta (Figs. 1 and 2).

2.5. Statistical analysis

The data were analyzed using SPSS version 22.0 with $P < 0.05$ indicating statistical significance. The data of normal distribution was tested by the independent samples *t*-test, and the data of non-normal distribution was tested by Mann-Whitney *U* test. The CT value differences at energy levels 50 keV, and from 80 to 100 keV (at 10 keV interval), and blood (water) concentration, and fat (water) concentration, and the NIC in arterial phase were compared between the liver abscesses and liver metastases using independent sample Mann-Whitney *U* test. The independent samples *t*-test was performed to compare the quantitative parameters NIC of venous and delay phase, and the CT value differences at energy levels 40 keV, 60 keV, 70 keV, and from 110 to 140 keV (at 10 keV interval), the slope (K) and Eff-Z between the

Table 1
The General Information of Patients with Liver Abscesses and Liver Metastases.

	Liver abscess (n = 28)	Liver metastasis (n = 45)	t	*P*
Sex	14(man)/11(women)	15(man)/11(women)	0.120	0.905
Age	60.40 ± 13.50	63.96 ± 13.69	−0.935	0.354
Lesion diameter	4.33 ± 1.73 cm	4.41 ± 2.26 cm	−0.397	0.691

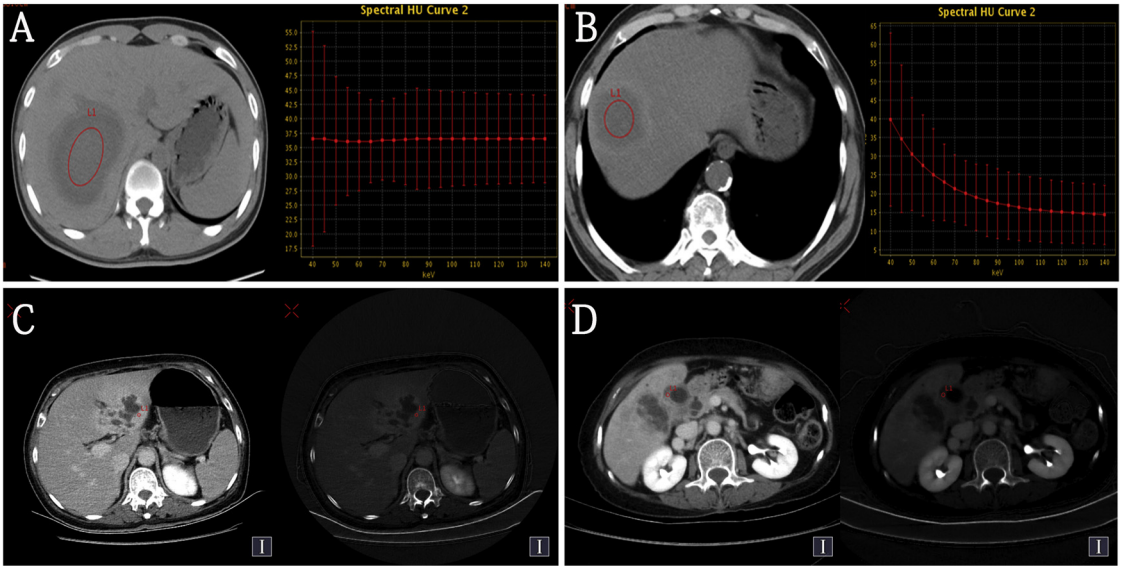

Fig. 1. (A) Unenhanced images in a 33-year-old man with liver abscess, after placing a circular ROI in the cystic component of the lesion, K value of the lesion on the spectral curve were 0.0002. (B) Unenhanced images in a 65-year-old man with liver metastasis, after placing a circular ROI in the cystic component of the lesion, K value of the lesion on the spectral curve were −0.2548. (C) Contrast-enhanced delay phase images in a 64-year-old women with liver abscess. The NIC of the wall in the lesion was 0.75. (D) Contrast-enhanced delay phase images in a 73-year-old women with liver metastasis. The NIC of the wall in the lesion was 0.30.

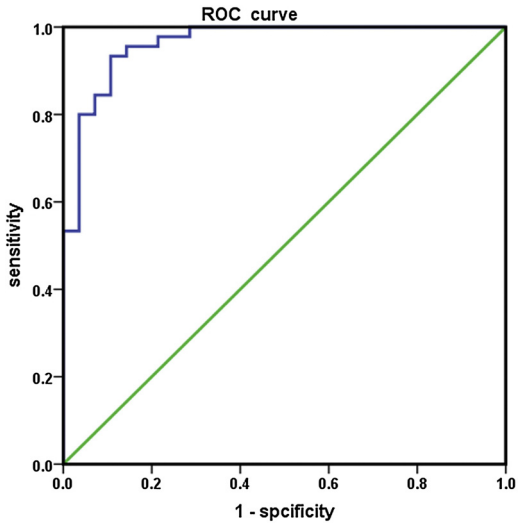

Fig. 2. The ROC curve of combination in differentiating liver metastases for liver abscesses.

liver abscesses and liver metastases. Monochromatic images for achieving the highest differences in the CT value, the slope (K), blood (water) concentration, fat (water) concentration, Eff-Z number and the NICs of enhanced three-phase images between the liver abscesses and liver metastases were analyzed by receiver operating characteristic (ROC) curves. The diagnostic capability was determined by calculating the area under the curve (AUC). Youden Index (Youden index = sensitivity + specificity-1) was calculated, and the best sensitivity and specificity were achieved by using the optimal diagnostic threshold. Finally, the combined two best quantitative parameters in the unenhanced and enhanced phases were fitted to logistic regression models to evaluate the predictive values. Qualitative CT imaging features were compared between the liver abscesses and liver metastases by the chi-squared tests.

Table 2
Qualitative CT Assessment of Lesions.

Features	Liver abscess (n = 28)	Liver metastasis (n = 45)	*P*
Love location			
Right hepatic lobe	7(25)	12(27)	0.875
Left hepatic lobe	21(75)	33(73)	0.875
Shape			
Regular	14(50)	36(80)	**0.007**
Irregular	14(50)	9(20)	**0.007**
Necrosis or cyst	28(100)	45(100)	1
Internal septa	13(29)	16(36)	0.356
Double target sign	12(27)	9(20)	**0.036**
Transient segmental enhancement of perilesional liver tissue	9(32)	8(18)	0.158
Enhancement pattern			
Rim enhancement	25(89)	36(80)	0.298
Washout during the portal venous phase	1(4)	2(4)	0.855
Delayed enhancement	27(96)	43(96)	0.855

Note: Data are number of lesions. Numbers in parentheses are percentages. *P* values were calculated using chi-squared test.

3. Results

3.1. Qualitative analysis

The CT features of the liver abscesses and liver metastases groups were analyzed and listed in Table 2. Double target sign was found in 12 (27%) of the 28 lesions of liver abscesses but only 9 (20%) of the 45 lesions of liver metastases ($P = 0.036$). Fourteen (50%) of the 28 lesions of liver abscesses showed regular shape, whereas 36 (80%) of the 45 lesions of liver metastases showed regular shape ($P = 0.007$).

3.2. Quantitative analysis

The differences in the quantitative parameters between the liver abscesses and liver metastases are listed in Tables 3 and 4. The mean CT values of the 40–140 keV unenhanced images (10 keV-interval) for liver abscesses were significantly lower than those for liver metastases

Table 3
Difference of Quantitative Parameters between Liver Abscesses and Liver Metastases.

	Liver Abscess (n = 28)	Liver Metastasis (n = 45)	t	*P*
CT Value^{40}	15.96 ± 15.38	31.52 ± 15.86	−3.732	**0.000**
CT Value^{60}	17.09 ± 9.34	25.54 ± 8.17	−3.523	**0.000**
CT Value^{70}	16.85 ± 8.59	23.46 ± 7.35	−3.256	**0.001**
CT Value^{110}	15.90 ± 9.44	20.00 ± 7.72	−2.530	**0.011**
CT Value^{120}	15.92 ± 9.50	19.76 ± 7.83	−2.422	**0.015**
CT Value^{130}	15.91 ± 9.54	19.58 ± 7.92	−2.360	**0.018**
CT Value^{140}	15.92 ± 9.60	19.40 ± 8.01	−2.258	**0.024**
Slope $^{(K)}$	−0.00 ± 0.15	−0.12 ± 0.17	−2.853	**0.004**
Eff-Z	7.55 ± 0.15	7.67 ± 0.17	−2.872	**0.004**
NIC $^{(venous)}$	0.46 ± 0.12	0.36 + 0.14	3.147	**0.002**
NIC $^{(delay)}$	0.72 ± 0.15	0.47 ± 0.14	7.395	**0.000**

($P < 0.05$). There were statistical significances in the slope (K) value, Eff-Z, fat (water) concentration and blood (water) concentration between liver abscesses and liver metastases ($P < 0.05$). The NIC value of the lesion walls in the venous and delay phase for liver abscesses were significantly higher than those for liver metastases ($P < 0.05$). There was no significant difference in the NIC value in the arterial phase between liver abscesses and liver metastases ($P > 0.05$).

The sensitivity, specificity for the differentiation of liver abscesses from liver metastases for each of the quantitative parameters are listed in Table 5. The CT value at 40 keV in the unenhanced image provided 0.761 of the area under the curve (AUC) in ROC with sensitivity of 71.4% and, specificity of 75.6% in differentiating liver abscess and tumor using the threshold value of 22.32HU for the CT value at 40 keV. The NIC in the delay phase had the greatest AUC of 0.899, indicating that it had the greatest differential ability. Using the optimal threshold of 0.62 for NIC, the sensitivity and specificity for differentiating liver abscesses from liver metastases in the delay phase was 78.6% and 88.9%, respectively. The combination of CT value at 40 keV in the unenhanced image and NIC in the delay phase improved the AUC value to 0.963. Using the optimal predicted probability threshold of 0.577, the sensitivity and specificity of this combination was 89.3% and 93.3%, respectively (Table 5, Fig. 2).

4. Discussion

Liver abscesses can be divided into inflammatory stage, early stage and pyogenic period pathologically. The abscess in the early stage or pyogenic period has partial or complete necrosis in the lesion. The necrotic cavity of liver abscess is filled with pus, which is a yellowish-brown, viscous fluid that consists of inflammatory cells, bacteria and necrotic tissue [9]. Liver tumors can be easily undergo cystic changes due to secretion of cystic fluid, internal bleeding, spontaneous liquefaction of necrosis or embolization [10]. When liver metastases develop central necrosis or cyst, the imaging characteristics are unusually atypical and can mimic liver abscesses. In these cases, all lesions had obvious liquefaction area. It's difficult to distinct between liver abscesses and liver metastases by using qualitative imaging features analyses alone. The present study was the first to investigate the application value of quantitative and qualitative analysis using CT spectral imaging in differentiating liver abscesses from liver metastases.

Table 5
Quantitative Parameters for Differential Diagnosis of Liver Abscesses and Liver Metastases.

	AUC	Maximum Youden Index	Threshold	Sensitivity	Specificity
CT Value^{40}	0.761	0.47	22.32	71.4%	75.6%
NIC $^{(delay)}$	0.899	0.68	0.62	78.6%	88.9%
Predicted Probability	0.963	0.83	0.58	89.3%	93.3%

According to the present study results, the CT values of the 40–140 keV unenhanced images (10 keV-interval), Eff-z, and blood (water) concentration for liver metastases were significantly higher than those for liver abscesses. The fat (water) concentration for liver metastases were significantly lower than those for liver abscesses. This can be attributed to the difference in the biochemical components of the cystic spaces [11]. The tumor cell division is more rapid and breaking down more lipids. It is relatively insufficient in the blood supply, and a small amount of hemorrhage is more likely to occur. The measured blood (water) concentration could be used to evaluate the trace bleeding of the lesions. The CT value could be used to evaluate the degree of necrosis of the lesions. Moreover, the tumor cell is active, leading to the density of the cystic area and the increase of mass attenuation coefficient. Therefore, the Eff-z of liver metastases was higher than liver abscesses. For medical diagnostic imaging, iodine and water are often selected as the basis pair for material decomposition images presentation because their atomic numbers span the range of atomic numbers for materials generally found in medical imaging and approximate those of soft tissue and iodinated contrast material to result in material-attenuation images that are intuitive to interpret [12]. For the walls of liver abscesses and liver metastases, iodine-based material decomposition images could be very sensitive, showing focal uptake of the iodinated contrast material. Furthermore, the measured iodine concentration in lesions might be a useful quantitative parameter that reflects the blood supply of lesions. The NIC in the venous and delay phase for liver abscesses were significantly higher than those for liver metastases. It is due to the delayed enhancement of liver abscesses and the peripheral cellular area with an increase in the number of blood vessels [13,14].

ROC curve analysis in the present study revealed that the CT value of the 40 keV monochromatic image in the plain phase and NIC in the delay phase had high sensitivity and specificity for differentiating liver abscesses from liver metastases. The best quantitative parameter was NIC in the delay phase and the threshold of 0.62 would yield a sensitivity and specificity of 78.6% and 88.9%, respectively. The combination of CT value of the 40 keV image in the plain phase and NIC in the delay phase had the greatest area under the curve (0.963) in ROC study. Using the optimal predicted probability threshold of 0.577, the sensitivity and specificity of this combination reached 89.3% and 93.3%, respectively.

Table 4
Difference of Quantitative Parameters between Liver Abscesses and Liver Metastases.

	Liver Abscess (n = 28)	Liver Metastasis (n = 45)	Z	*P*
CT Value^{50}	17.34 (10.71, 25.35)	28.03 (17.73, 34.37)	−3.710	**0.000**
CT Value^{80}	16.55 (11.41, 21.01)	22.34 (18.66, 27.54)	−3.222	**0.001**
CT Value^{90}	16.38 (10.91, 20.14)	21.52 (17.21, 25.63)	−2.938	**0.003**
CT Value^{100}	16.58 (10.48, 20.44)	21.24 (16.76, 24.28)	−2.634	**0.008**
Fat (water) Concentration	−84.91 (−135.44, 34.42)	355.97 (−148.65, 570.27)	−2.802	**0.005**
Blood (water) Concentration	−128.06 (−253.52, −59.91)	539.79 (249.50, 1068.31)	−2.768	**0.000**
NIC $^{(arterial)}$	0.13 (0.09, 0.20)	0.10 (0.08, 0.14)	−1.724	0.085

Use of these quantitative parameters in the dual-energy spectral CT imaging to differentiate liver abscesses from liver metastases in patients could help to avoid further MR imaging, follow-up CT, or biopsy, which can result in additional costs, delayed treatment, and unnecessary anxiety. Moreover, we found that the use of the quantitative parameters, namely the CT value of the 40 keV images in the plain phase and NIC in the delay phase, showed higher accuracy than other parameters. The binary combination of these two parameters showed greatest area under the ROC curve.

The present study did have some limitations. First, the research needs to be verified by collecting a large number of patients. Second, all lesions have obvious liquefaction area. Further research in solid mass is required. Third, in our study, we limited the study to distinguish liver abscesses from liver metastases, not the different types of metastatic tumors. However, the properties of metastasis are influenced by the histological type of the primary tumor. In the futre, we would need to collect a large number of lesions of distinguish between different types of metastases.

In conclusion, the quantitative parameters in dual-energy spectral CT provide high diagnostic accuracy in differentiating liver abscesses from liver metastases.

Ethics approval

This study was approved by the institutional review board at the corresponding author's institution.

Consent for publication

Not applicable.

Availability of data and material

The raw data cannot be made freely available because of privacy restrictions.

Funding

Program for Training Capital Science and Technology Leading Talents (Z181100006318003).

Conflict of interests

The authors declare that they have no conflict of interests.

References

[1] D. Glambelluca, F. Panzuto, E. Giambelluca, et al., The "double target sign" in liver abscess, Abdom. Radiol. (NY) (March) (2018).
[2] H.S. Alsaif, S.K. Venkatesh, D.S. Chan, et al., CT appearance of pyogenic liver abscesses caused by Klebsiella pneumoniae, Radiology 260 (1) (2011) 123–138.
[3] C. Schmid-Tannwald, C.M. Schmid-Tannwald, J.N. Morelli, et al., Role of diffusion-weighted MRI in differentiation of hepatic abscesses from non-infected fluid collections, Clin. Radiol. 69 (7) (2014) 687–694.
[4] M.M. Hammer, V.M. Mellnick, C.A. Raptis, et al., Peripheral restricted diffusion: a common appearance of hepatic abscesses, J. Comput. Assist. Tomogr. 39 (6) (2015) 890–895.
[5] A. Chen, A. Liu, J. Liu, et al., Application of dual-energy spectral CT imaging in differential diagnosis of bladder cancer and benign prostate hyperplasia, Medicine (Baltim.) 95 (52) (2016) e5705.
[6] Y. Ju, A. Liu, Y. Dong, et al., The value of nonenhanced single-source dual-energy CT for differentiating metastases from adenoma in adrenal glands, Acad. Radiol. 22 (7) (2015) 834–839.
[7] J.E. Kim, H.O. Kim, K. Bae, et al., Differentiation of small intrahepatic mass-forming cholangiocarcinoma from small liver abscess by dual source dual-energy CT quantitative parameters, Eur. J. Radiol. 92 (2017) 145–152.
[8] S.Y. Choi, Y.K. Kim, J.H. Min, et al., The value of gadoxetic acid-enhanced MRI for differentiation between hepatic microabscesses and metastases in patients with periampullary cancer, Eur. Radiol. 27 (10) (2017) 4383–4393.
[9] Y. Yu, L. Guo, C. Hu, et al., Spectral CT imaging in the differential diagnosis of necrotic hepatocellular carcinoma and hepatic abscess, Clin. Radiol. 69 (12) (2014) 517–524.
[10] S. De Rave, S.M. Hussain, A liver tumor as an incidental finding: differential diagnosis and treatment, Scand. J. Gastroenterol. Suppl. 236 (2002) 81–86.
[11] J.H. Chan, E.Y. Tsui, S.H. Luk, et al., Diffusion-weighted MR imaging of the liver: distinguishing hepatic abscess from cystic or necrotic tumor, Abdom. Imaging 26 (2) (2001) 161–165.
[12] D. Muenzel, G.C. Lo, H.S. Yu, et al., Material density iodine images in dual-energy CT: detection and characterization of hypervascular liver lesions compared to magnetic resonance imaging, Eur. J. Radiol. 95 (October) (2017) 300–306.
[13] C.L. Wanq, X.J. Guo, S.B. Qiu, et al., Diagnosis of bacterial hepatic abscess by CT, Hepatobiliary Pancreat. Dis. Int. 6 (3) (2007) 271–275.
[14] H.J. Park, S.H. Kim, K.M. Janq, et al., Differentiating hepatic abscess from malignant mimickers: value of diffusion-weighted imaging with an emphasis on the periphery of the lesion, J. Magn. Reson. Imaging 38 (6) (2013) 1333–1341.